

## Article

# Effect of W Content on Microstructure and Properties of Laser Cladding CoCrFeNi HEA Coating

Fangyan Luo , Tuchuan Yang, Yang Zhao, Zhengye Xiong  and Jiang Huang \*

School of Electronics and Information Engineering, Guangdong Ocean University, Zhanjiang 524088, China; m18922863861@163.com (F.L.); yangyang202131@163.com (T.Y.); 18530183037@163.com (Y.Z.); xiongzhenye@139.com (Z.X.)

\* Correspondence: huangjiang@gdou.edu.cn

**Abstract:** The 316L SS surfaces were prepared with CoCrFeNi HEA/W-composite coatings using the laser cladding technique with various mass fractions of W. The mass fractions of W were 10, 20, 30, and 40%. The microstructure of the HEA/W-composite coatings was investigated using a variety of characterization methods. According to the results, the samples were in the BBC phase. In the SEM images, a solid-liquid bonding layer was observed, which indicates the samples had good metallurgical bonding. The W particles prevented the orderly growth of the HEA grains, and a significant refinement of the grains around the W particles occurred. The lattice constants measured by XRD mapping indicate that adding W particles to CoCrFeNi HEA leads to lattice distortion. The hardness of the HEA/W coatings was substantially higher than the substrate and the pure CoCrFeNi coating by hardness measurements and was greatest at a W content of 40%. The hardness of the HEA/W coatings was significantly increased compared to the substrate and the pure CoCrFeNi coating by hardness measurements and was greatest at a W content of 40%. The HEA/W coating was tested for electrochemical corrosion, and a 10% mass fraction of W achieved the highest level of corrosion resistance.

**Keywords:** laser cladding; microstructure; HEA; microhardness; corrosion resistance



**Citation:** Luo, F.; Yang, T.; Zhao, Y.; Xiong, Z.; Huang, J. Effect of W Content on Microstructure and Properties of Laser Cladding CoCrFeNi HEA Coating. *Coatings* **2023**, *13*, 1301. <https://doi.org/10.3390/coatings13081301>

Academic Editor: Stefano Caporali

Received: 6 July 2023

Revised: 20 July 2023

Accepted: 21 July 2023

Published: 25 July 2023



**Copyright:** © 2023 by the authors. Licensee MDPI, Basel, Switzerland. This article is an open access article distributed under the terms and conditions of the Creative Commons Attribution (CC BY) license (<https://creativecommons.org/licenses/by/4.0/>).

## 1. Introduction

Advanced surface modification technologies can improve the surface properties and prolong the life of materials, making them irreplaceable in today's manufacturing industry. There are many surface modification techniques [1]. Laser melting technology, as a surface modification technique, has a fast heating and cooling process. This means it has a lower dilution rate and a smaller heat affected zone. Another benefit of laser cladding technology is that it is inexpensive and pollution-free. These advantages make laser cladding technology suitable for use in the petroleum, chemical, aviation, mechanical engineering, and shipbuilding industries [2–5].

Over the past 20 years, high-entropy alloys (HEAs) have undergone fast development as new alloys. HEAs have a new design concept and are generally solid solutions consisting of four or more metal components [6–10]. HEAs have a simple solid solution structure and essentially face-centered cubic (FCC) or body-centered cubic (BCC) phases. HEA has attracted a lot of interest from academics because of its favorable properties [11–13]. However, limited by the production level, HEAs are mainly utilized as powders or thin flakes. This does not meet the requirements of manufacturing or industrial applications. Therefore, the leading research today uses HEA powders as surface coating materials when preparing metal surfaces using laser cladding technology, which results in materials with the excellent unique properties of HEAs.

CoCrFeNi HEA is a kind of FCC-phase HEA with excellent corrosion resistance. The alloy system contains Co and Cr, both of which improve the corrosion resistance of

HEAs [14]. It has sparked a lot of research interest recently. The proportion of elements in the CoCrFeNi HEA powder found by Shu et al. [15] and Zhang et al. [16] has a significant impact on the coating's characteristics. Zhu Q et al. [17] found that the preparation of CoCrFeNi HEA coatings utilizing the laser cladding process did not show any composition segregation and the elements were uniformly distributed, which improved the coatings' ability to resist corrosion as a consequence. CoCrFeNi HEA coatings were created by Zhang Q et al. [18] using both high-speed laser cladding and regular laser cladding. The findings revealed that the high-speed laser cladding produced superior CoCrFeNi HEA coatings in terms of performance. Laser cladding was employed by Wang W R et al. [19] to prepare (CoCrFeNi)<sub>95</sub>Nb<sub>5</sub> coatings at different laser energy densities and observed their corrosion resistance properties. This study showed that both hardness and corrosion resistance decreased as the density of the laser energy rose, demonstrating the controllability of the laser cladding technique for preparing high-performance HEA coatings. Many scholars have also studied the performance studies of composite coatings prepared by adding other elements to CoCrFeNi HEA, such as metallic elements, intermetallic compounds, and ceramic metals. According to Guo Y X et al. [20], adding in situ TiN reinforcing particles to CoCrFeNi HEA powders increased the wear resistance and hardness of the composite coatings. Qi C et al. [21] prepared coatings of prepared Al<sub>x</sub>CoCrFeNi HEA by the laser cladding technique and found that by increasing the mass fraction of Al, the HEA coatings showed the microhardness increased when the crystal structure changed from FCC to FCC with BCC and BCC. By using the vacuum inductive melting technique, Lin S et al. [22] created high-entropy CoCrFeNi alloy matrix composites with micron- and nanosized TiC and SiC particles. The findings revealed that the FCC structure of the composite was preserved and its mechanical characteristics were enhanced. In a recent study, Hang J et al. [23] discovered that WC ceramic particles could increase the hardness and corrosion resistance of CoCrFeNi HEA coatings while preserving the FCC phase. There are few reports on the preparation of CoCrFeNi HEA by adding W particles, a refractory metal particle, to CoCrFeNi HEA by the laser cladding technique and observing its microstructure and various features. In our previous study [23], pure CoCrFeNi coatings had lower hardness and improved corrosion resistance compared to 316L SS. Therefore, we have fabricated CoCrFeNi HEA composite coatings with mass fractions of W of 10, 20, 30, 40 and 0% on the surface of 316L SS using conventional laser cladding techniques. The microstructure, hardness, and corrosion resistance of the HEA/W-composite coatings with various W mass fractions were investigated.

## 2. Experimental Processes

### 2.1. Material and Coating Preparation

In preparation for the experiments, we first prepared 316L SS as substrates, CoCrFeNi HEA powder, and W particles. Figure 1 shows the microscopic morphology and distribution maps of the CoCrFeNi HEA powder and the spherical W particles. Tables 1 and 2 show the chemical composition of 316L SS and the CoCrFeNi HEA powder. The dimensions of the 316L SS steel were 100 mm (length) × 50 mm (width) × 2 mm (thickness). The 316L SS surface had been polished using sandpaper. Afterwards, it was purified with ethanol. The spherical W particles were mixed with CoCrFeNi HEA powder using a CZ0001 planetary ball mill for 2 h. Afterwards, it was dried in the oven for 2 h. Table 3 shows the labeling methods for HEA/W-composite coatings prepared from different mass fractions of W. Based on our experience from previous experiments and research work, we used the XL-F2000W fiber continuous laser processing system (model: XL-F2000W, manufacturer: Maxphotonics Co., Ltd., Shenzhen, China) for laser cladding and the production of multi-track coatings. The parameters were: maximum output power of 2 kw, circular Gaussian beam, spot diameter of 2.5 mm, laser beam wavelength of 1080 nm, laser scanning speed of 700 mm/min, overlap rate of 50%, and the defocus was +2 mm. The experiments were carried out in a pre-set powder mode by using a standard mold and setting the powder thickness to 1 mm.

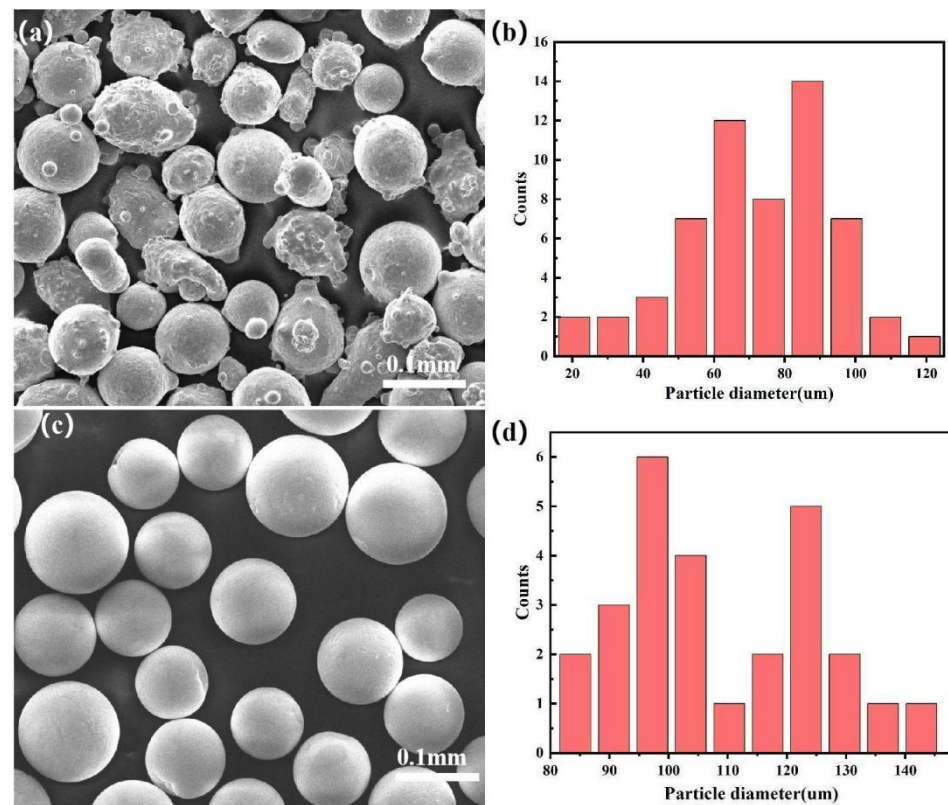


**Figure 1.** SEM morphology: (a) CoCrFeNi HEA powders; (b) CoCrFeNi HEA powder distribution map; (c) spherical W particles; (d) spherical W particle distribution map.

**Table 1.** Chemical composition of 316L SS (mass fraction, %).

Cr	Ni	Mn	MO	Si	Fe
16–18	10–14	2	2–3	1.5	Bal.

**Table 2.** Chemical composition of the CoCrFeNi HEA powder (mass fraction, %).

Cr	Ni	Co	Fe
22.98	26.07	26.16	24.79

**Table 3.** Coating numbers with different W mass fractions.

Label of Coating	Content of W/(Mass Fraction, %)
A	CoCrFeNi HEA + 10% W
B	CoCrFeNi HEA + 20% W
C	CoCrFeNi HEA + 30% W
D	CoCrFeNi HEA + 40% W
E	CoCrFeNi HEA

## 2.2. Test Methods

After preparing the samples, the HEA/W-composite coating was cut to a size of 10 mm (length)  $\times$  10 mm (width)  $\times$  2 mm (thickness) using a wire cutter, after which it was subjected to microstructural analysis. The microstructure was analyzed using a scanning electron microscope (SEM, FEI, Quanta 250 FEG, Hillsboro, OR, USA). The chemical compositions of the samples were determined with an energy-dispersive spectrometer (EDS). An X-ray diffractometer (XRD, XRD-6100, Shimadzu, Kyoto, Japan) was used for

detecting the phase composition of composite coatings, characterized by a scanning speed of  $7^\circ/\text{min}$  and a selection of scanning angles from  $20^\circ$  to  $80^\circ$ . Using a Vickers hardness tester, the microhardness of the cladding and substrate was determined (model: MHVD-1000AT, manufacturer: Yizong precision instrument Co., Ltd., Shanghai, China) with a load of 200 g for 10 s. The corrosion resistance were measured using an electrochemical workstation (CHI660E, Chen Hua Instruments, Shanghai, China). The corrosion resistance of the samples was measured in a 3.5% NaCl solution at room temperature with a test voltage scan range of  $-1.3\text{ V}$  to  $+0.5\text{ V}$ .

### 3. Results and Discussion

#### 3.1. Microstructure and EDS Mapping Analysis

The cross-sectional morphology of HEA/W-composite coatings with various W mass fractions is depicted in Figure 2. It was observed that spherical W particles were formed in the lower part of the coating. As the mass fraction of W increased, the spherical W particles formed at the bottom of the coating also increased. The primary cause is because CoCrFeNi HEA powder has a lower density than W particles, where the density of CoCrFeNi alloy is  $8.040\text{ g/cm}^3$  and the W particle density is  $19.3\text{ g/cm}^3$ , so that W particles will settle at the bottom of the coating under the effect of gravity. At the same time, a uniform dispersion of W particles in the coating was observed. This shows that the convection effect caused both the W particles and the HEA powder to melt evenly in the high-temperature molten pool. Figure 2e simulates the effects of gravity and convection on W particles during the laser cladding process.

We chose sample B for the EDS mapping test in order to further confirm that the spherical particles created in the lower part of the coating were W particles. The findings are displayed in Figure 3. The EDS mapping test results for sample B showed that the spherical particles were W particles. Additionally, Co, Cr, Fe, and Ni were all dispersed equally throughout the coating, and there was no component segregation.

SEM images showed the microstructure of the surface and cross-sectional dendrite morphology of the HEA/W-composite coating. Laser cladding is a typical non-equilibrium solidification process. According to the compositional cooling criterion [24], the direction of the greatest heat flux loss has an impact on the morphology of the microstructure created during laser cladding. The temperature gradient (G) and solidification rate (R) are two critical factors that determine the crystal structure of HEA [24–26]. Rapid melting occurs during the laser cladding process; the powder on the surface of the substrate melts rapidly and spreads, ultimately solidifying through the heat dissipation of the substrate. This process is indicated by the high temperature of the powder subjected to laser action but the low temperature of the substrate. Therefore, G is large. In the solid solution interface, G is large, resulting in a very large G/R. As a result, crystal growth rate is lower than crystal nucleation rate, and crystals can form planar crystals by growing in the direction of heat dissipation [27]. At this point, planar crystals are generated at the solid–liquid bonding layer, which is the interface between the substrate and coating, as in Figure 4b, as the solid–solution interface progresses quickly. This suggests that the coating layer and the substrate have a good metallurgical bond [1]. Previous studies have confirmed that planar growth and dendritic formation indicate the formation of metal bonds [28,29].

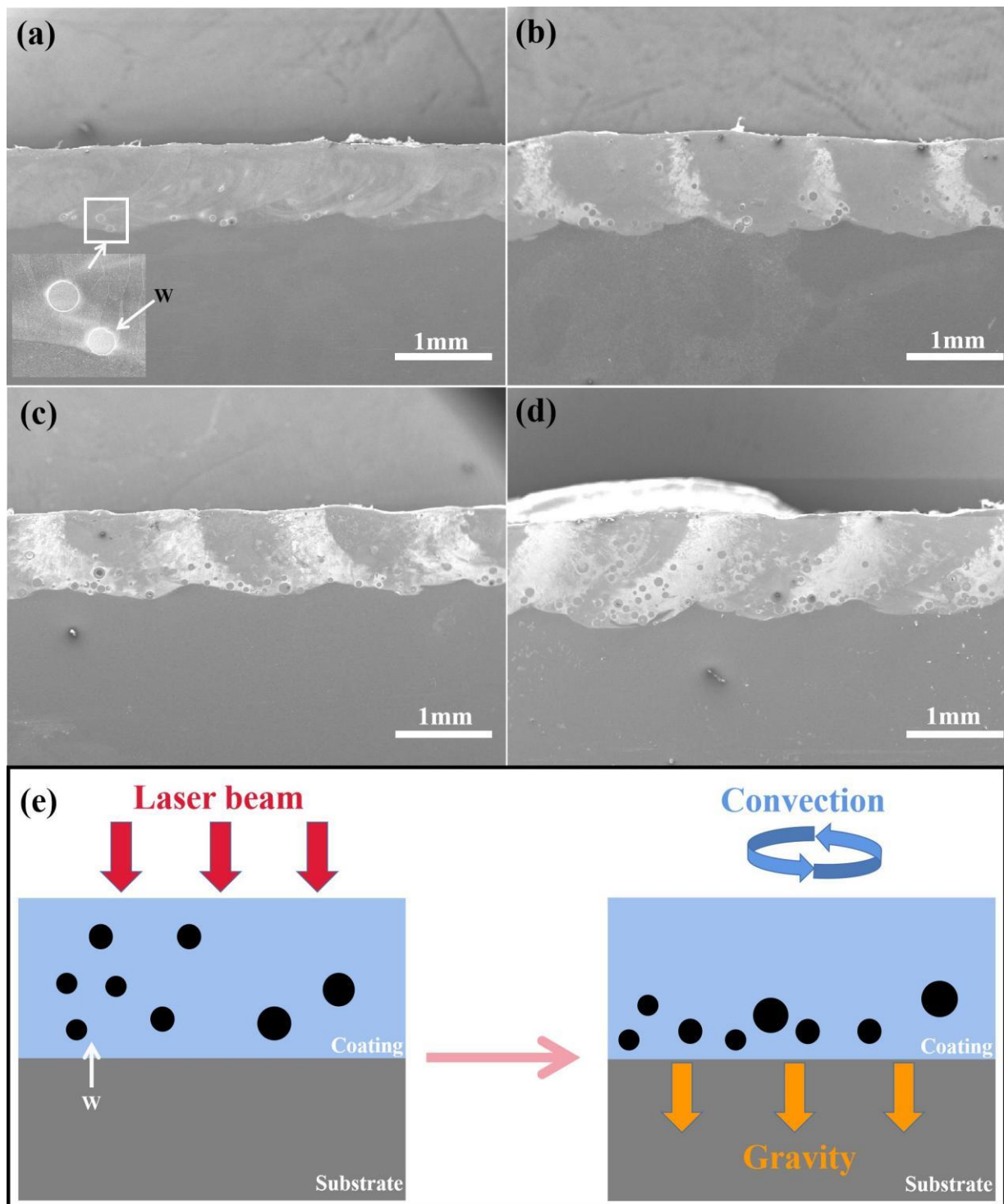


**Figure 2.** SEM micrographs of each HEA/W coatings. (a) Sample A; (b) sample B; (c) sample C; (d) sample D; (e) gravity and convection model.

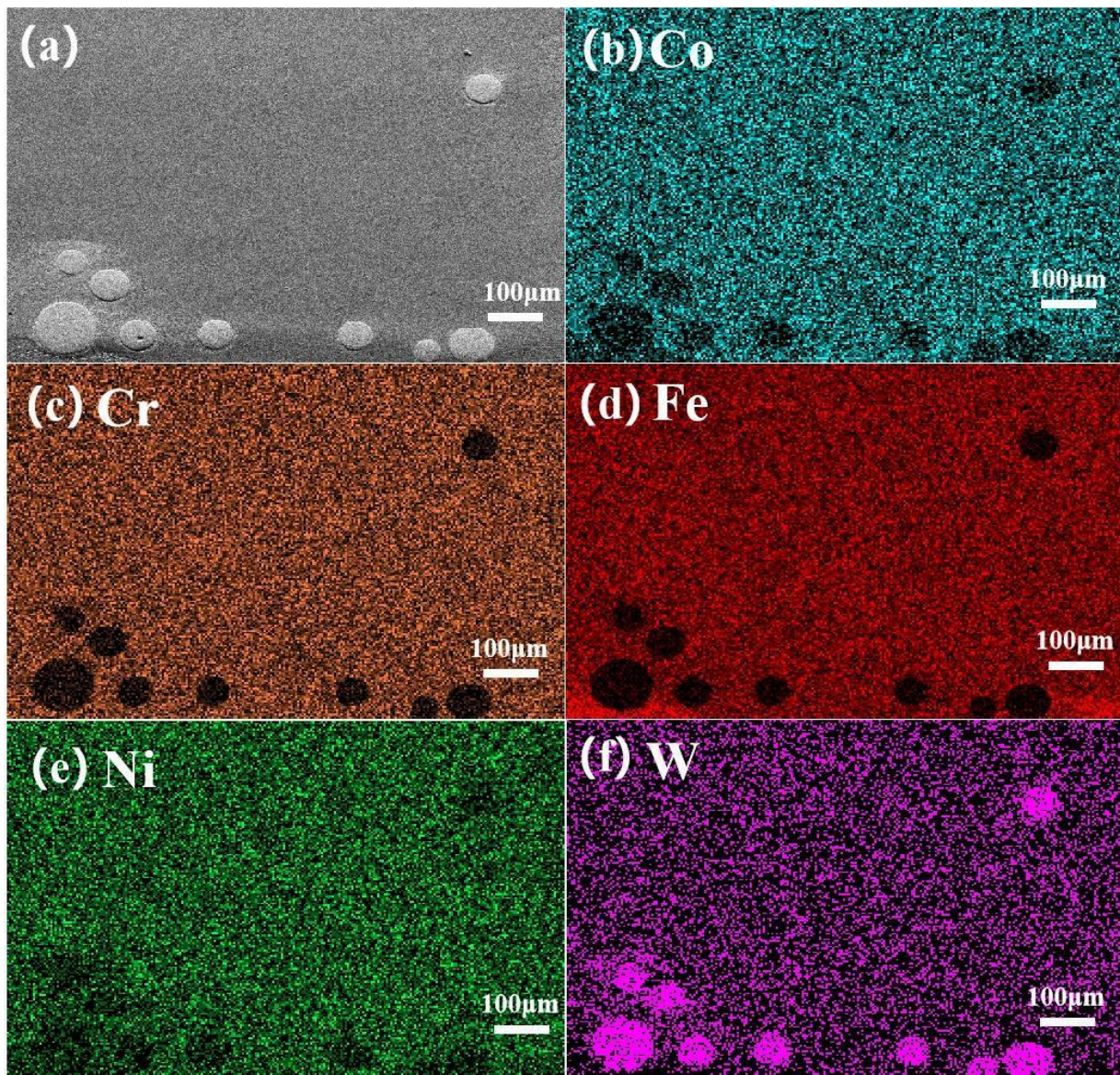


**Figure 3.** EDS mapping of sample B's element distribution. (a) SEM micrographs of sample B; (b) Co; (c) Cr; (d) Fe; (e) Ni; (f) W.

One can observe, in Figure 4c,e, where columnar crystals growing in a vertical direction were formed in the coating in the area without W particles. By observing Figure 4d,f, it can be seen that a significant refinement of grain size occurred in the region around the W particles with the increasing mass fraction of W. This is because when the melt near the unmelted W particles solidified, the heat flow was directed to the residual W particles in the molten metal at low temperatures. This created microregional directional growth [30], further refining the tissue, and exhibiting regional grain refinement, making the coating more stable. In addition, the W particles acted as a barrier to the growth of columnar crystals. This is mostly because the large particles added to HEA caused some lattice distortion, which limited grain growth [31].

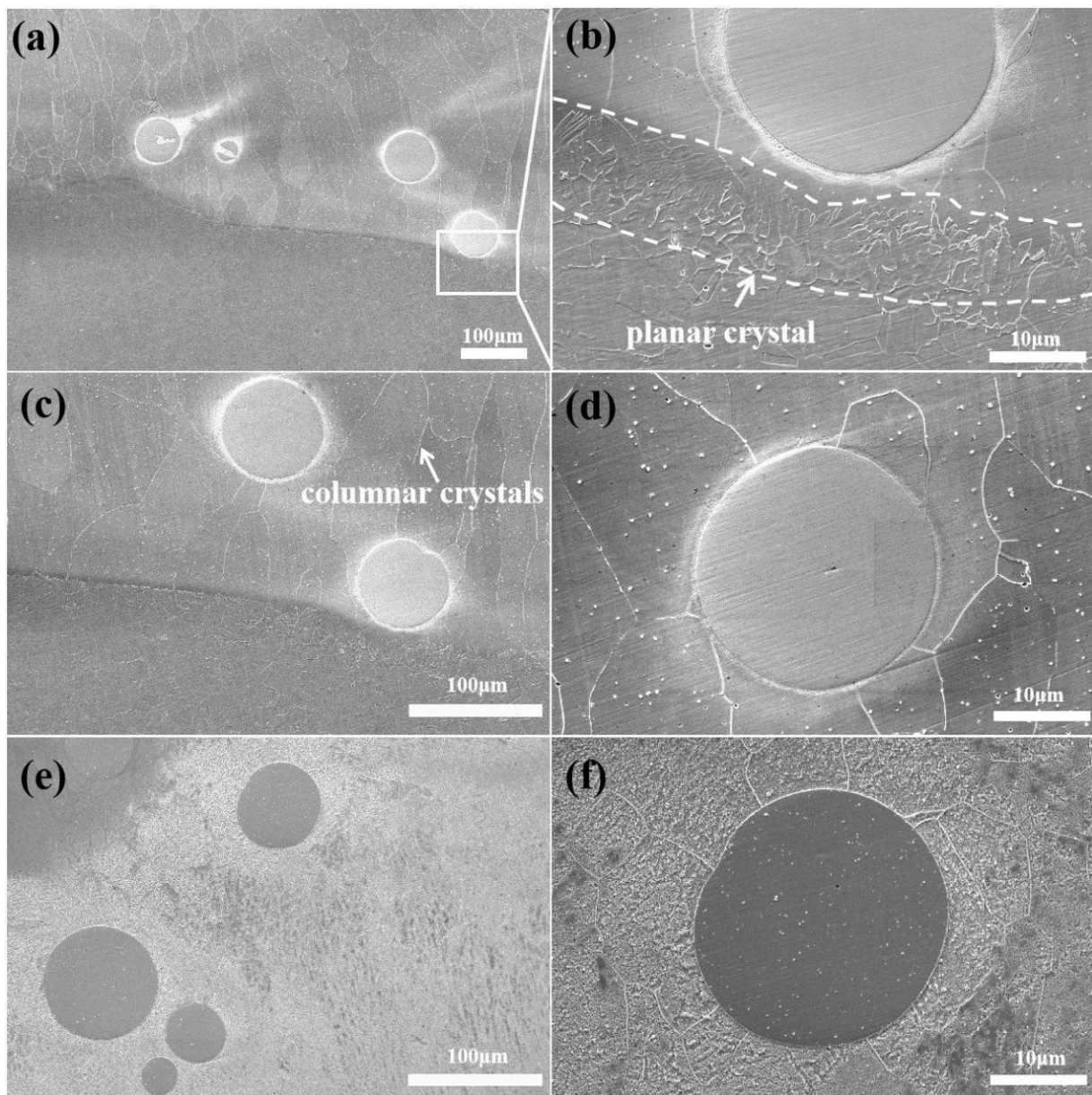


**Figure 4.** SEM micrographs. (a) SEM micrographs of bottom of sample A; (b) magnification of bottom coating section; (c) SEM micrographs of sample A; (d) magnification of W particle-coating section of sample A; (e) SEM micrographs of sample D; (f) magnification of W particle-coating section of sample D.

### 3.2. Phase Composition

As the mass fraction of W grew, the composite coatings changed to the BCC phase, as illustrated in Figure 5 from the XRD image. The laser cladding process encourages Ni diffusion in the alloy system. At the same time, when the W concentration rises, alloying of Ni is encouraged. (PDF#65-7753, PDF#65-7752). This is one of the reasons why it is important that the composite coatings are BCC phase.

Notably, no other alloy compounds containing W appeared in the XRD pattern. This indicates that no interaction between HEA and W occurred during the laser cladding. A leftward shift in the position of the main peak with the increasing mass fraction of W was observed in the magnified image of the main peak from XRD. A literature review showed [32,33] that, according to Bragg's law: the increase in lattice spacing is the primary cause of the main peak's location shifting to the left. Figure 6 shows the lattice constants

for each coating as calculated by XRD. It was evident that when the W mass fraction rose, the lattice constant rose as well. This indicates that the lattice distortion of CoCrFeNi HEA occurred after adding W [34], which resulted in a rise in the constant of the lattice and a movement of the main peak location to the left. On the other hand, with increased W concentration, it was noticed that the diffraction peaks of the main peaks widened, which was ascribed to microscopic stresses brought on by lattice deformation without a specific direction and magnitude, which resulted in irregular changes in the crystal plane spacing [32].

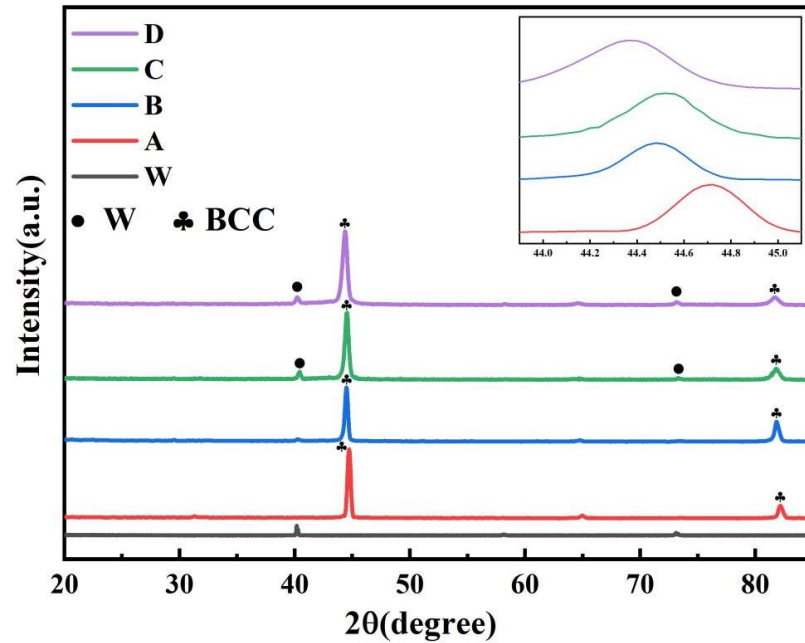


Figure 5. XRD pattern of HEA/W laser cladding coating.

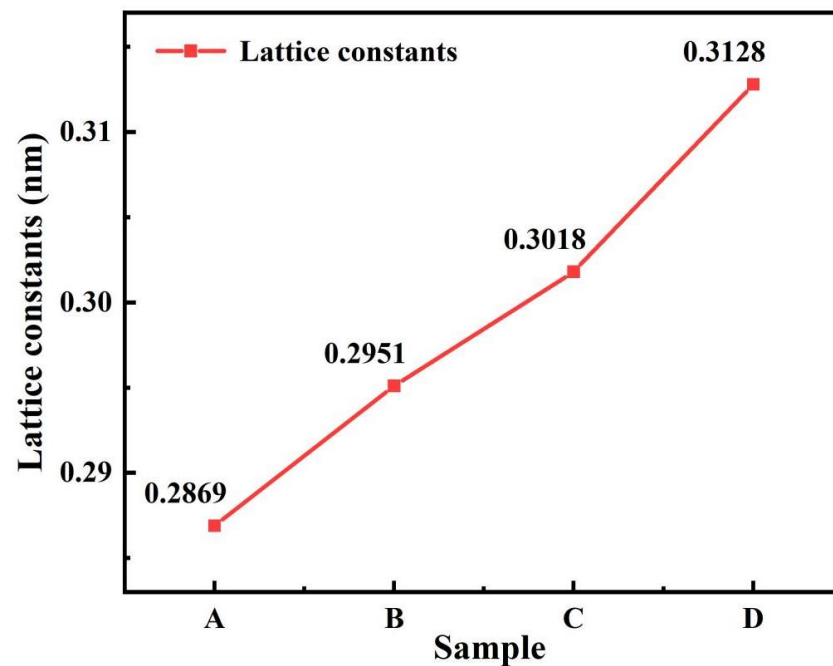


Figure 6. Lattice constants of CoCrFeNi HEA/W coatings.

### 3.3. Microhardness

Figure 7a shows the hardness distribution of the HEA/W-composite coatings and the pure CoCrFeNi HEA coating cross-section for the 316L substrate, heat-affected zone (HAZ) and composite-coating regions. Figure 7b illustrates the results of calculating the average hardness of the 316L substrate region, each composite coating region, and the pure CoCrFeNi HEA coating. The average microhardness values of the HEA/W-composite coatings with 10, 20, 30 and 40% W content, the pure CoCrFeNi HEA coating and 316L substrate, were 599.04, 668.70, 685.68, 743.86, 174.98 and 209.48 HV, respectively. This suggests that when the W component grows, the microhardness of HEA/W-composite coatings increases as well. Furthermore, the coatings' average microhardness was 2.78 to 3.45 times greater than that of the 316L substrate. It is important to note that the 316L substrate's average hardness is higher than that of pure CoCrFeNi HEA coating. However, the average hardness of HEA/W-composite coatings with W particles added was significantly higher than pure CoCrFeNi HEA coating and the 316L substrate. When the W component was 10%, solid-solution strengthening took on a significant role. The addition of large particles of W to the HEA powder caused a certain amount of lattice distortion. By hindering grain growth, it raised the coating layer's hardness and resistance to dislocation movement [35]. When the W content was 20 to 40%, W-rich phases started to be found in the XRD examination of HEA/W. At this point, the W particles acted as reinforcing phase particles, impeding the effect of dislocation slip. This left a dislocation ring, exerting reverse stress on the dislocation source and increasing the hardness. This is known as Orowan strengthening [36]. At the same time, observation of the SEM cross-sectional morphology of HEA/W showed that the W particles were uniformly dispersed and precipitated at the bottom of the HEA/W coating, which also impeded dislocation movement and thus enhanced the coatings' microhardness. This is referred to as dispersion strengthening and precipitated hardening [37,38]. The SEM scans showed a sizable amount of grain refinement surrounding the W grains. The finer the grain size, the smaller the number of dislocations in the dislocation population, resulting in a smaller stress concentration and thus a harder material. At this point, dispersion strengthening, precipitation strengthening, solid-solution strengthening, and grain refinement simultaneously boosted the coatings' microhardness.

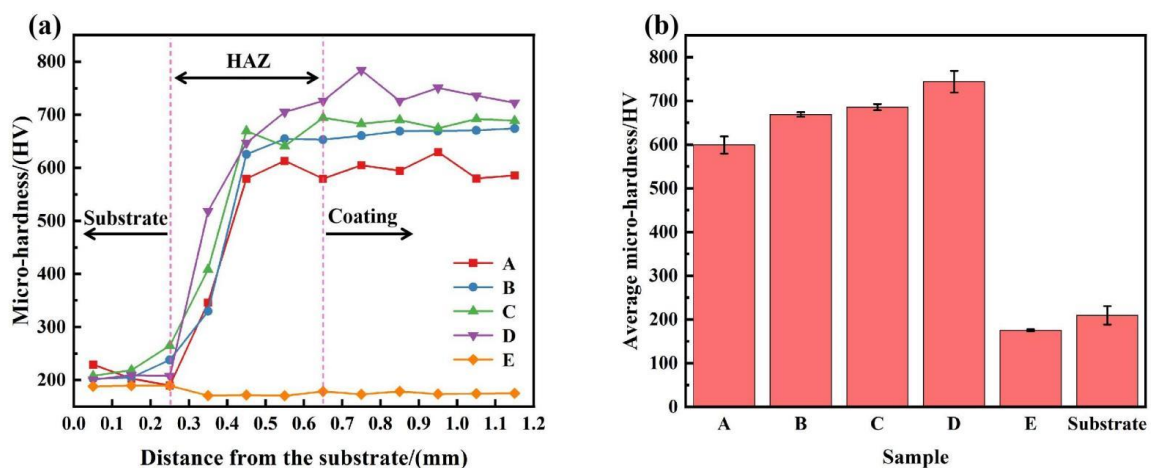


Figure 7. (a) The HEA/W-composite coatings' hardness distributions; (b) average microhardness of HEA/W coating and 316L substrate.

### 3.4. Corrosion Resistance

We utilized a three-electrode cell to examine the corrosion properties of the HEA/W-composite coating at room temperature. For each sample, the experiment was run at least three times to assure accuracy. The test samples were stated as being 1 mm × 1 mm in size. After 30 min of immersion in a 3.5% NaCl solution, the samples' electrochemical

characteristics were examined. Figure 8 shows the Tafel curves for each sample using the Tafel slope extrapolation method in Table 4 [39]. According to corrosion guidelines, the corrosion potential ( $E_{\text{corr}}$ ) depicts the coating's propensity for corrosion. If the  $E_{\text{corr}}$  is more positive, the corrosion tendency is smaller. The corrosion rate of the coating decreased with decreasing corrosion current density ( $I_{\text{corr}}$ ). Generally, a smaller  $I_{\text{corr}}$  and a higher  $E_{\text{corr}}$  mean a higher corrosion resistance [40,41]. As shown in Table 4, the molten cladding layer A had the highest corrosion potential ( $E_{\text{corr}} = -0.446$  V) and a low corrosion current density ( $I_{\text{corr}} = 1.884 \times 10^{-8}$  A/cm<sup>2</sup>). All HEA/W-composite coatings had a higher corrosion potential and a lower corrosion current density compared to the substrate and all HEA/W-composite coatings had higher corrosion potentials compared to the pure CoCrFeNi HEA coating. Consequently, it can be concluded that the HEA/W-cladding layer leads to an improvement in the corrosion resistance of the substrate and the pure CoCrFeNi HEA coating.

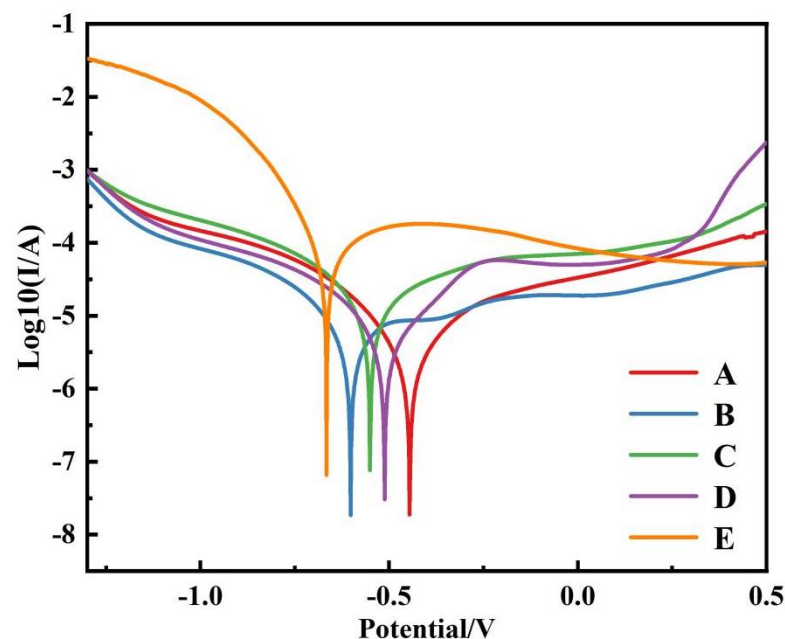


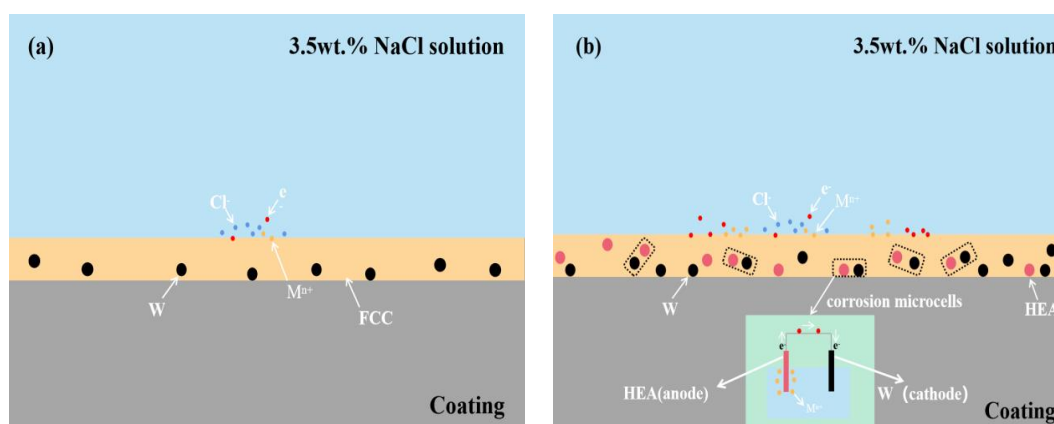
Figure 8. The potentiodynamic polarization evolution curves of HEA/W composite coatings.

Table 4. The samples'  $I_{\text{corr}}$  and  $E_{\text{corr}}$ .

Materials	$E_{\text{corr}}$ (V/SCE)	$I_{\text{corr}}$ (A/cm <sup>2</sup> )
A	−0.446	$1.884 \times 10^{-8}$
B	−0.602	$1.834 \times 10^{-8}$
C	−0.551	$7.569 \times 10^{-8}$
D	−0.512	$3.033 \times 10^{-8}$
E	−0.666	$6.549 \times 10^{-8}$
316L SS [23]	−0.705	$8.184 \times 10^{-7}$

According to Table 4, the composite coatings' resistance to corrosion deteriorates when an excessive amount of W was added. This is due to the formation of corrosion microcells with HEA as the anode and W as the cathode. The area effect of corrosion microcells [42,43] supports this: as the W content increases, the cathodic area subsequently increases, the cathodic current density increases, more HEAs are used as anodes, and the number of corrosion microcells formed increases, which promotes electrochemical corrosion. Therefore, adding too much W will reduce the coatings' corrosion resistance. Figure 9a,b illustrate the microscopic corrosion mechanism of the composite coating. As the mass fraction of W increases, the cathode area increases, and more corrosion microcells

are formed, similar to Figure 9b. This accelerates the electron transfer of the positive metal elements in the HEA and results in a decline in the composite coatings' corrosion resistance.



**Figure 9.** HEA/W corrosion mechanism diagram. (a) Sample A; (b) samples B, C and D.

#### 4. Conclusions

- (1) The HEA/W-composite coatings were prepared on 316L SS substrates with different mass fractions of W. Gravity and convection factors caused the W particles to be evenly distributed at the bottom of the coatings, according to SEM and EDS examinations. Large W particles were added to the HEA powder, which resulted in lattice distortion and grain refinement in the HEA.
- (2) After the W particles were added, the HEA/W-composite coatings changed to the BCC structure. Moreover, throughout the laser cladding process, the W particles did not interact with the CoCrFeNi HEA powder. As the W content rose, the primary peak in the XRD pattern moved to the left. The primary cause of this is that the increase in the size of the W particles leads to lattice distortion, which increases the lattice spacing and thus shifts the main peak to the left.
- (3) Compared with the 316L SS and pure CoCrFeNi coating, the HEA/W-composite coatings' hardness increased dramatically. The composite coating with a mass fraction W of 40% achieved the highest average hardness. Among the main strengthening methods are solid solution strengthening, dispersion strengthening, grain refinement simultaneously, and precipitation strengthening.
- (4) Electrochemical experiments showed that the HEA/W-composite coatings had an increased corrosion potential compared to the 316L SS substrate and the pure CoCrFeNi coating. This indicates that the HEA/W coating with added W possesses better corrosion resistance. Of them, the 10% HEA/W-composite coating showed the best corrosion resistance.

**Author Contributions:** Conceptualization, J.H.; methodology, Y.Z.; software, F.L.; validation, J.H., F.L. and T.Y.; formal analysis, Z.X.; investigation, F.L.; resources, J.H.; data curation, J.H.; writing—original draft preparation, Y.Z.; writing—review and editing, J.H.; visualization, J.H.; supervision, F.L.; project administration, J.H.; funding acquisition, J.H. All authors have read and agreed to the published version of the manuscript.

**Funding:** Supported by the national natural science foundation projects (No. 62073089), and Laser processing team project of Guangdong Ocean University (No. CCTD201823).

**Institutional Review Board Statement:** Not applicable.

**Informed Consent Statement:** Not applicable.

**Data Availability Statement:** Not applicable.

**Conflicts of Interest:** The authors declare no conflict of interest.

## References

1. Xiao, Q.; Sun, W.L.; Yang, K.X.; Xing, X.F.; Chen, Z.H.; Zhou, H.N.; Lu, J. Wear mechanisms and micro-evaluation on WC particles investigation of WC-Fe composite coatings fabricated by laser cladding. *Surf. Coat. Technol.* **2021**, *420*, 127341. [[CrossRef](#)]
2. Ning, J.Q.; Sievers, D.E.; Garmestani, H.; Liang, S.Y. A Analytical modeling of insitute formation of part and substrate in laser cladding additive manufacturing of Inconel 625. *J. Manuf. Process.* **2020**, *49*, 135–140. [[CrossRef](#)]
3. Liu, H.; Tan, C.K.I.; Wei, Y.; Lim, S.H.; Lee, C.J. Laser cladding and interface evolutions of inconel 625 alloy on low alloy steel substrate upon heat and chemical treatments. *Surf. Coat. Technol.* **2020**, *404*, 126607. [[CrossRef](#)]
4. Zhu, L.; Xue, P.; Lan, Q.; Meng, G.; Ren, Y.; Yang, Z.; Xu, P.; Liu, Z. Recent research and development status of laser cladding: A review. *Opt. Laser Technol.* **2021**, *138*, 106915. [[CrossRef](#)]
5. Li, H.C.; Wang, D.G.; Hu, C.; Dou, J.H.; Yu, H.J.; Chen, C.Z.; Gu, G.C. Microstructure mechanical and biological properties of laser cladding derived CaO-SiO<sub>2</sub>-MgO system ceramic coatings on titanium alloys. *Appl. Surf. Sci.* **2021**, *548*, 149296. [[CrossRef](#)]
6. Yeh, J.W.; Chen, S.K.; Lin, S.J.; Gan, J.Y.; Chin, T.S.; Shun, T.T.; Tsau, C.H.; Chang, S.Y. Nanostructured high-entropy alloys with multiple principal elements: Novel alloy design concepts and outcomes. *Adv. Eng. Mater.* **2004**, *6*, 299–303. [[CrossRef](#)]
7. Yeh, J.W.; Chang, S.Y.; Hong, Y.D.; Chen, S.K.; Lin, S.J. Anomalous decrease in X-ray diffraction intensities of Cu-Ni-Al-Co-Cr-Fe-Si alloy systems with multi-principal elements. *Mater. Chem. Phys.* **2007**, *103*, 41–46. [[CrossRef](#)]
8. Ye, Y.F.; Wang, Q.; Lu, J.; Liu, C.T.; Yang, Y. High-entropy alloy: Challenges and prospects. *Mater. Today* **2016**, *19*, 349–362. [[CrossRef](#)]
9. Ye, Y.F.; Wang, Q.; Lu, J.; Liu, C.T.; Yang, Y. Design of high entropy alloys: A single parameter thermodynamic rule. *Scr. Mater.* **2015**, *104*, 53–55. [[CrossRef](#)]
10. Zhang, Y.; Zuo, T.T.; Tang, Z.; Gao, M.C.; Dahmen, K.A.; Liaw, P.K.; Lu, Z.P. Microstructures and properties of high-entropy alloys. *Prog. Mater. Sci.* **2014**, *61*, 1–93. [[CrossRef](#)]
11. Gludovatz, B.; Hohenwarter, A.; Catoor, D.; Chang, E.H.; George, E.P.; Ritchie, R.O. A fracture-resistant high-entropy alloy for cryogenic applications. *Science* **2014**, *345*, 1153–1158. [[CrossRef](#)]
12. Lee, C.P.; Chen, Y.Y.; Hsu, C.Y.; Yeh, J.W.; Shih, H.C. The effect of boron on the corrosion resistance of the high entropy alloys Al<sub>0.5</sub>CoCrCuFeNiBx. *J. Electrochem. Soc.* **2017**, *154*, 424–430. [[CrossRef](#)]
13. Senkov, O.N.; Senkova, S.V.; Woodward, C. Effect of aluminum on the microstructure and properties of two refractory high entropy alloys. *Acta Mater.* **2014**, *68*, 214–228. [[CrossRef](#)]
14. Shang, C.; Axinte, E.; Sun, J.; Li, X.; Li, P.; Du, J.; Qiao, P.; Wang, Y. CoCrFeNi(W1 x Mox) high-entropy alloy coatings with excellent mechanical properties and corrosion resistance prepared by mechanical alloying and hot pressing sintering. *Mater. Des.* **2017**, *117*, 193e202. [[CrossRef](#)]
15. Shu, F.Y.; Yang, B.; Dong, S.Y.; Zhao, H.Y.; Xu, B.S.; Xu, F.J.; Liu, B.; He, P.; Feng, J.C. Effects of Fe-to-Co ratio on microstructure and mechanical properties of laser clad FeCoCrBNiSi high-entropy alloy coatings. *Appl. Surf. Sci.* **2018**, *450*, 538–544. [[CrossRef](#)]
16. Zhang, H.F.; Yan, H.L.; Yu, H.; Ji, Z.W.; Hu, Q.M.; Jia, N. The effect of Co and Cr substitutions for Ni on mechanical properties and plastic deformation mechanism of FeMnCoCrNi high entropy alloys. *J. Mater. Sci. Technol.* **2020**, *48*, 146–155. [[CrossRef](#)]
17. Zhu, Q.; Liu, Y.; Zhang, C.Y. Laser cladding of CoCrFeNi high-entropy alloy coatings: Compositional homogeneity towards improved corrosion resistance. *Mater. Lett.* **2022**, *318*, 132133.
18. Zhang, Q.; Han, B.; Li, M.Y.; Chen, Z.B.; Hu, C.Y.; Jia, C.X. Comparison of CoCrFeNi coatings prepared via high-speed laser cladding and normal laser cladding on microstructure and properties. *Intermetallics* **2023**, *153*, 107795. [[CrossRef](#)]
19. Wang, W.R.; Qi, W.; Zhang, X.L.; Yang, X.; Xie, L.; Li, D.Y.; Xiang, Y.H. Superior corrosion resistance-dependent laser energy density in (CoCrFeNi)<sub>95</sub>Nb<sub>5</sub> high entropy alloy coating fabricated by laser cladding. *Int. J. Miner. Metall. Mater.* **2021**, *28*, 888–897. [[CrossRef](#)]
20. Guo, Y.X.; Shang, X.J.; Liu, Q.B. Microstructure and properties of in-situ TiN reinforced laser cladding CoCr<sub>2</sub>FeNiTi<sub>x</sub> high-entropy alloy composite coatings. *Surf. Coat. Technol.* **2018**, *344*, 353–358.
21. Chao, Q.; Guo, T.T.; Jarvis, T.; Wu, X.H.; Hodgson, P.; Fabijanic, D. Direct laser deposition cladding of Al<sub>x</sub>CoCrFeNi high entropy alloys on a high-temperature stainless steel. *Surf. Coat. Technol.* **2017**, *332*, 440–451. [[CrossRef](#)]
22. Shen, L.; Zhao, Y.; Li, Y.; Wu, H.; Zhu, H.G.; Xie, Z.H. Synergistic strengthening of FeCrNiCo high entropy alloys via micro-TiC and nano-SiC particles. *Mater. Today Commun.* **2020**, *26*, 101729. [[CrossRef](#)]
23. Huang, J.; Zhu, Z.K.; Wang, H.; Li, K.Y.; Shi, W.Q.; Jiao, T.W. Effect of WC Content on Microstructure and Properties of CoCrFeNi HEA Composite Coating on 316L Surface via Laser Cladding. *Materials* **2023**, *16*, 2706. [[CrossRef](#)]
24. Rutter, J.W.; Chalmers, B. A prismatic substructure formed during solidification of metals. *Can. J. Phys.* **1953**, *31*, 15–39. [[CrossRef](#)]
25. Peng, Y.B.; Zhang, W.; Li, T.C. Microstructures and mechanical properties of FeCoCrNi high entropy alloy/WC reinforcing particles composite coatings prepared by laser cladding and plasma cladding. *Int. J. Refract. Met. Hard Mater.* **2019**, *84*, 105044. [[CrossRef](#)]
26. Shen, F.M.; Tao, W.; Li, L.Q.; Zhou, Y.D.; Wang, W.; Wang, S.L. Effect of microstructure on the corrosion resistance of coatings by extreme high speed laser cladding. *Appl. Surf. Sci.* **2020**, *517*, 146085. [[CrossRef](#)]
27. Peng, Y.B.; Zhang, W.; Li, T.C.; Zhang, M.Y.; Liu, B.; Liu, Y.; Wang, L.; Hu, S.W. Effect of WC content on microstructures and mechanical properties of FeCoCrNi high entropy alloy/WC composite coatings by laser cladding and plasma cladding. *Surf. Coat. Technol.* **2020**, *385*, 125326.

28. Chen, H.H.; Xu, C.Y.; Chen, J. Microstructure and phase transformation of WC/Ni60B laser cladding coatings during dry sliding wear. *Wear* **2008**, *264*, 487–493.
29. Zhang, D.W.; Zhang, X.P. Laser cladding of stainless steel with Ni–Cr<sub>3</sub>C<sub>2</sub> and Ni–WC for improving erosive–corrosive wear performance. *Surf. Coating. Technol.* **2005**, *190*, 212–217. [[CrossRef](#)]
30. Liu, X.M. Mechanism and control of the nick-based alloy WC laser clad layer microstructure. *Appl. Laser* **2006**, *5*, 299–302+306.
31. Deng, C.; Wang, C.; Chai, L.J.; Wang, T.; Luo, J. Mechanical and chemical properties of CoCrFeNiMo<sub>0.2</sub> high entropy alloy coating fabricated on Ti6Al4V by laser cladding. *Intermetallics* **2022**, *144*, 107504. [[CrossRef](#)]
32. Jiang, C.P.; Zhang, J.; Chen, Y.N.; Hou, Z.M.; Zhao, Q.Y.; Li, Y.; Zhu, L.X.; Zhang, F.Y.; Zhao, Y.Q. On enhancing wear resistance of titanium alloys by laser clad WC-Co composite coatings. *Int. J. Refract. Met. Hard Mater.* **2022**, *107*, 105902. [[CrossRef](#)]
33. Gu, Z.; Xi, S.Q.; Sun, C.F. Microstructure and properties of laser cladding and CoCr<sub>2.5</sub>FeNi<sub>2</sub>Ti<sub>x</sub> high-entropy alloy composite coatings. *J. Alloys Compd.* **2020**, *819*, 152986. [[CrossRef](#)]
34. Li, Y.T.; Fu, H.G.; Ma, T.J.; Wang, K.M.; Yang, X.J.; Lin, J. Microstructure and wear resistance of AlCoCrFeNi-WC/TiC composite coating by laser cladding. *Mater. Charact.* **2022**, *194*, 112479. [[CrossRef](#)]
35. Roy, A.; Sreeramagiri, P.; Babuska, T.; Krick, B.; Ray, P.K.; Balasubramanian, G. Lattice distortion as an estimator of solid solution strengthening in high-entropy alloys. *Mater. Char.* **2021**, *172*, 110877.
36. Liu, X.Y.; Zhang, L.; Xu, Y. Microstructure and mechanical properties of grapheme reinforced Fe<sub>50</sub>Mn<sub>30</sub>Co<sub>10</sub>Cr<sub>10</sub>, high-entropy alloy composites synthesized by MA and SPS. *Appl. Phys. A Mater. Sci. Process.* **2017**, *123*, 567. [[CrossRef](#)]
37. Chen, P.; Yang, C.; Li, S.; Attallah, M.M.; Yan, M. In-situ alloyed, oxide-dispersionstrengthened CoCrFeMnNi high entropy alloy fabricated via laser powder bed fusion. *Mater. Des.* **2020**, *194*, 108966. [[CrossRef](#)]
38. Haftlang, F.; Kim, H.S. A perspective on precipitation-hardening high-entropy alloys fabricated by additive manufacturing. *Mater. Des.* **2021**, *211*, 110161. [[CrossRef](#)]
39. Xu, W.; Hu, S.W.; Li, W.H. Corrosion monitoring for prestressed concrete cylinder pipe spigot with combined use of Tafel extrapolation and surface acoustic wave methods. *Constr. Build. Mater.* **2022**, *337*, 127572.
40. Rodriguez, A.A.; Tylczak, J.H.; Gao, M.C.; Jablonski, P.D.; Detrois, M.; ZiomekMoroz, M.; Hawk, J.A. Effect of molybdenum on the corrosion behavior of high entropy alloys CoCrFeNi<sub>2</sub> and CoCrFeNi<sub>2</sub>Mo<sub>0.25</sub> under sodium chloride aqueous conditions. *Adv. Mater. Sci. Eng.* **2018**, *2018*, 3016304. [[CrossRef](#)]
41. Yu, K.D.; Zhao, W.; Li, Z.; Guo, N.; Xiao, G.C.; Zhang, H. High-temperature oxidation behavior and corrosion resistance of in-situ TiC and Mo reinforced AlCoCrFeNi-based high entropy alloy coatings by laser cladding. *Ceram. Int.* **2023**, *49*, 10151–10164. [[CrossRef](#)]
42. Zhang, H.; Liu, Y.; Bai, X.; Zhao, W.; Zhang, P.; Rao, W.F. Laser cladding highly corrosion-resistant nano/submicron ultrafine-grained Fe-based composite layers. *Surf. Coating. Technol.* **2021**, *424*, 127636. [[CrossRef](#)]
43. Sun, S.; Liu, H.; Hao, J.; Yang, H. Microstructural evolution and corrosion behavior of CoCrFeNiAlxMn(1 – x) dual-phase high-entropy alloy coatings prepared by laser cladding. *J. Alloys Compd.* **2021**, *886*, 161251. [[CrossRef](#)]

**Disclaimer/Publisher’s Note:** The statements, opinions and data contained in all publications are solely those of the individual author(s) and contributor(s) and not of MDPI and/or the editor(s). MDPI and/or the editor(s) disclaim responsibility for any injury to people or property resulting from any ideas, methods, instructions or products referred to in the content.